



Photoluminescence properties, excellent thermal stability and energy transfer in Ce³⁺ and Tb³⁺ co-doped Sr₃Gd₂(BO₃)₄ phosphors

Xiaoxuan Fan^a, Xiaoyuan Sun^{a,*}, Chunmiao Liu^a, Wanlu Tian^a, Min Li^a, Yongshi Luo^b, Chunlei Wu^c

^a Department of Physics, Changchun Normal University, Changchun, 130032, China

^b State Key Laboratory of Luminescence and Application, Changchun Institute of Optics, Fine Mechanics and Physics, Chinese Academy of Science, Changchun, 130033, China

^c Faculty of Science, Mudanjiang Normal University, Mudanjiang, 157012, China

ARTICLE INFO

Keywords:

Luminescence
Highly efficient energy transfer
White LEDs
Green phosphor

ABSTRACT

Sr₃Gd₂(BO₃)₄: Ce³⁺, Sr₃Gd₂(BO₃)₄: Tb³⁺ and Sr₃Gd₂(BO₃)₄: Ce³⁺, Tb³⁺ phosphors were synthesized through conventional high temperature solid state reaction method. Phase purity, crystal structure, photoluminescence properties, and lifetime of the samples were analyzed in detailed. Sr₃Gd₂(BO₃)₄: Ce³⁺ showed a bright blue broad emission band, which was attributed to 4f → 5d transitions of the Ce³⁺ ions, and it exhibited two broad excitation bands ranged from 200 nm to 400 nm. For all Sr₃Gd₂(BO₃)₄: Tb³⁺ samples, under ultraviolet excitation bands of 240 nm, four emissions peaked at 490 nm, 544 nm, 585 nm and 623 nm appeared, due to the ⁵D₄ → ⁷F_J (J = 6, 5, 4, 3) transitions of Tb³⁺ ions. For the Sr₃Gd₂(BO₃)₄: Ce³⁺, Tb³⁺ phosphors, the lifetime of the samples were analyzed, which showed the presence of energy transfer between the Ce³⁺ and Tb³⁺. The energy transfer efficiency from Ce³⁺ ions to Tb³⁺ ions reached 98.37%. When the temperature reached 443 K, the luminescence intensity reached 88% of the initial value. Finally, a white LED was fabricated by using a 365 nm near ultraviolet LED chip combined with BaMgAl₁₀O₁₇: Eu²⁺ (blue), Sr₃Gd_{0.91}(BO₃)₄: 0.09Ce³⁺, 1.0 Tb³⁺ (green), and CaAlSiN₃: Eu²⁺ (red) phosphors. The color coordinates was (0.40, 0.42); correlated color temperature was 3721 K; color rendering index was 91.1. The results showed that the Sr₃Gd₂(BO₃)₄: Ce³⁺, Tb³⁺ green phosphors were suitable for white LEDs.

1. Introduction

White light-emitting diodes (LED) had the characteristics of energy conservation, environmental protection and high efficiency. It was the excellent light source that purchased by all of mankind. LEDs promoted a new type of lighting revolution [1–7]. Current commercial white lighting was generally obtained by a combination of blue-emitting InGaN chips and yellow-emitting rare-earth phosphors [8,9]. Another better approach was that near ultraviolet chips combined with red, blue and green phosphors. This method had high color rendering index and excellent prospects, which attracted many researchers to develop novel and efficient phosphors that could be excited by ultraviolet light [10–13].

As one of the most promising rare earth activators, Tb³⁺ ions showed excellent green emission at around 545 nm, which originated from the ⁵D₄ → ⁷F₅ transition of Tb³⁺ ions. The 4f → 4f transition of Tb³⁺ ions was

forbidden. Therefore, Tb³⁺ ions had very weak absorption in the ultraviolet region [14–17]. In order to solve this problem, Ce³⁺ ions usually used as an effective sensitizer for the Tb³⁺ emission, because Ce³⁺ ions allowed the 4f → 5d transition. There was highly efficient energy transfer from Ce³⁺ ions to Tb³⁺ [18–22].

At present, the energy transfer from Ce³⁺ ions to Tb³⁺ ions have been reported. For instance, Ca₂YHf₂Al₃O₁₂: Ce³⁺, Tb³⁺, LaAl_{2.03}B₄O_{10.54}: Ce³⁺, Tb³⁺, Ba₂Lu₅B₅O₁₇: Ce³⁺, Tb³⁺, Ba₃Y₂(B₂O₅)₃: Ce³⁺, Tb³⁺ etc. [23–30]. A. Shyichuk reported the Sr₃Gd₂(BO₃)₄: Tb³⁺ samples, the materials could be used in high-frame rate 3D PDP screens [31]. In this paper, we prepared the Sr₃Gd₂(BO₃)₄: Ce³⁺, Sr₃Gd₂(BO₃)₄: Tb³⁺ and Sr₃Gd₂(BO₃)₄: Ce³⁺, Tb³⁺ phosphors. We analyzed the crystal structure, spectral properties, thermal stability and life time of the samples. The results indicated that Sr₃Gd₂(BO₃)₄: Ce³⁺, Tb³⁺ green phosphors have potential application in ultraviolet excited white LEDs.

* Corresponding author.

E-mail address: sxueyuan@163.com (X. Sun).

<https://doi.org/10.1016/j.jlumin.2021.118594>

Received 25 July 2021; Received in revised form 7 November 2021; Accepted 9 November 2021

Available online 16 November 2021

0022-2313/© 2021 Elsevier B.V. All rights reserved.

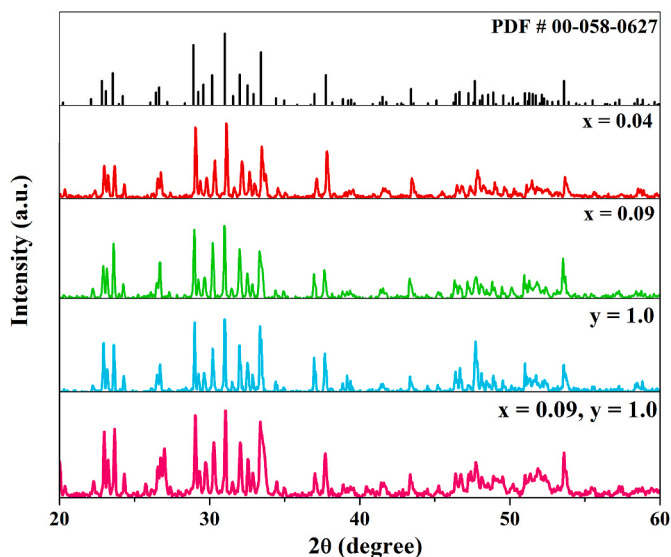


Fig. 1. XRD patterns for SGBO: 0.04 Ce³⁺, SGBO: 0.09 Ce³⁺, SGBO: 1.0 Tb³⁺ and SGBO: 0.09Ce³⁺, 1.0 Tb³⁺ phosphors.

2. Experimental

The phosphors of Sr₃Gd_(2-x)(BO₃)₄: xCe³⁺ (named as SGBO: Ce³⁺) (x = 0.01, 0.02, 0.03, 0.04, 0.05, 0.06, 0.075, 0.1, 0.15, 0.2), Sr₃Gd_(2-x)(BO₃)₄: xTb³⁺ (named as SGBO: Tb³⁺) (x = 0.05, 0.1, 0.25, 0.5, 0.75,

1.0, 1.25, 1.5) and Sr₃Gd_(1.91-y)(BO₃)₄: 0.09Ce³⁺, yTb³⁺ (named as SGBO: 0.09Ce³⁺, yTb³⁺) (y = 0.2, 0.4, 0.6, 0.8, 1.0, 1.2, 1.4, 1.6, 1.8) were synthesized by high-temperature solid state reaction technique. The starting materials, CeO₂ (99.99%; Sinopharm Chemistry Reagent Co., Ltd), Tb₄O₇ (99.995%; Quannan County New Resources Rare Earth Co., Ltd), H₃BO₃ (AR; Sinopharm Chemistry Reagent Co., Ltd), SrCO₃ (AR; Sinopharm Chemistry Reagent Co., Ltd), Gd₂O₃ (99.999%; Quannan County New Resources Rare Earth Co., Ltd) were weighed according to the stoichiometric ratio. All of the raw materials were grinded 40 min with an agate mortar. Then mixtures were placed in corundum crucibles, added crucible covers, and then put them into the muffle furnace. The samples were sintered at 1100 °C for 6 h under CO reducing atmosphere. After sintered, the products were slowly cooled to room temperature. The samples were ground again into the powders for subsequent use.

The crystal phase of all the phosphor samples was identified by using X-ray powder diffraction (XRD) analysis with a Rigaku D/MAX-RB diffractometer. The emission and excitation spectra were measured by the fluorescence spectrometer (FL-4600, Tokyo, Japan) equipped with a 150 W Xe lamp. The Tb³⁺ fluorescence lifetime was measured by Tektronix-TD digital oscilloscope. The Ce³⁺ fluorescence lifetime was measured by FLS980 fluorescence spectrometer. Temperature-dependent emission spectra were recorded on the Raman Spectrometer (JY-Horiba labRam infinity). The performance of the packaged LED was measured by the Ocean Optics micro fiber spectrometer USB4000. Internal Quantum Efficiency (IQE) and External Quantum Efficiency (EQE) value were measured by F-7000 spectrometer based on the integrating sphere method, and an integrating sphere coated by BaSO₄ was used as the attachment.

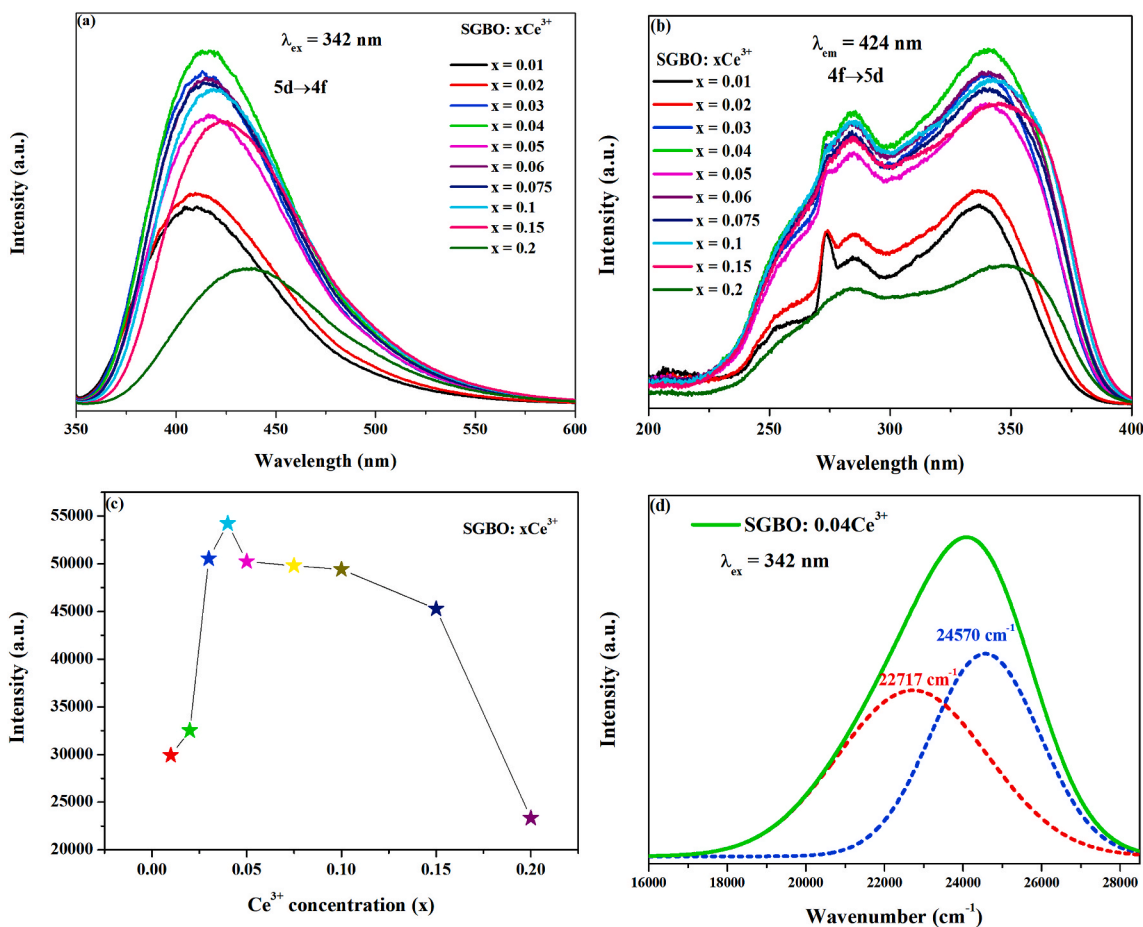


Fig. 2. (a) The emission spectra of SGBO: xCe³⁺ phosphors. (b) The excitation spectra of SGBO: xCe³⁺ phosphors. (c) Dependence of photoluminescence intensity on Ce³⁺ concentration. (d) The emission spectrum of SGBO: 0.04Ce³⁺ phosphor was analyzed by Gaussian fitting.

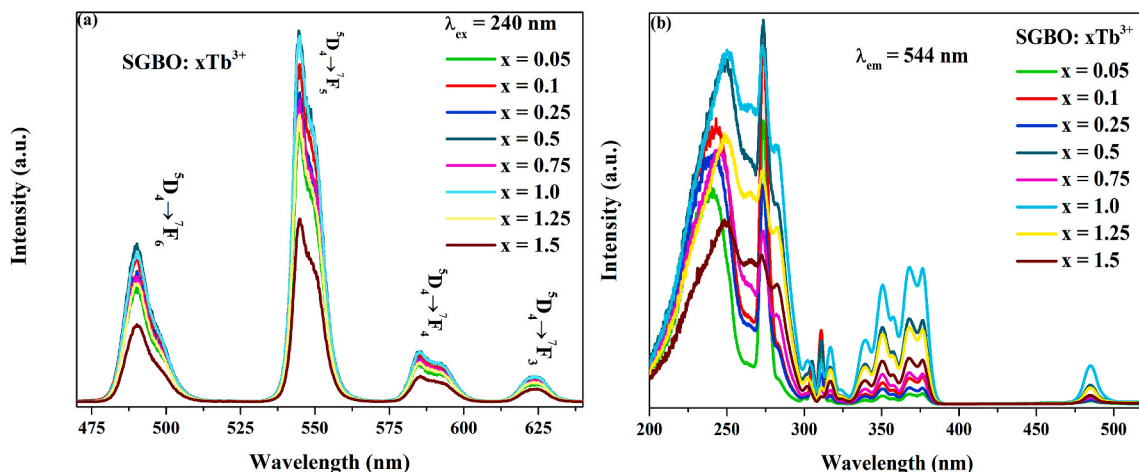


Fig. 3. (a) The emission spectra of SGBO: xTb³⁺ phosphors ($\lambda_{ex} = 240$ nm) and (b) the excitation spectra of SGBO: xTb³⁺ phosphors ($\lambda_{em} = 544$ nm).

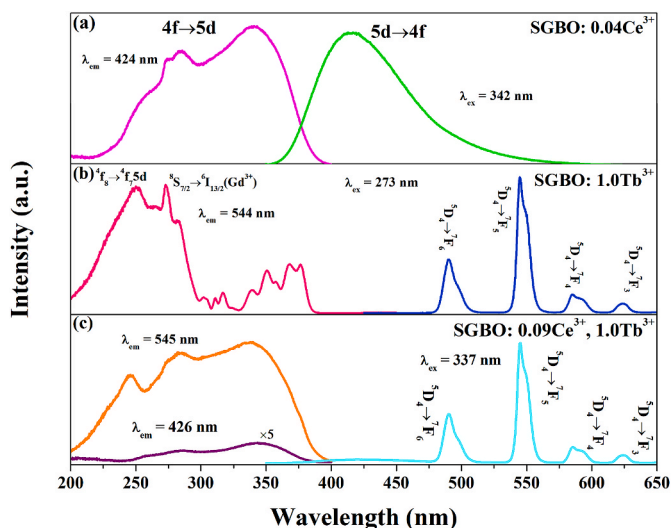


Fig. 4. Emission and excitation spectra of (a) SGBO: 0.04Ce³⁺, (b) SGBO: 1.0 Tb³⁺ and (c) SGBO: 0.09Ce³⁺, 1.0 Tb³⁺ phosphors.

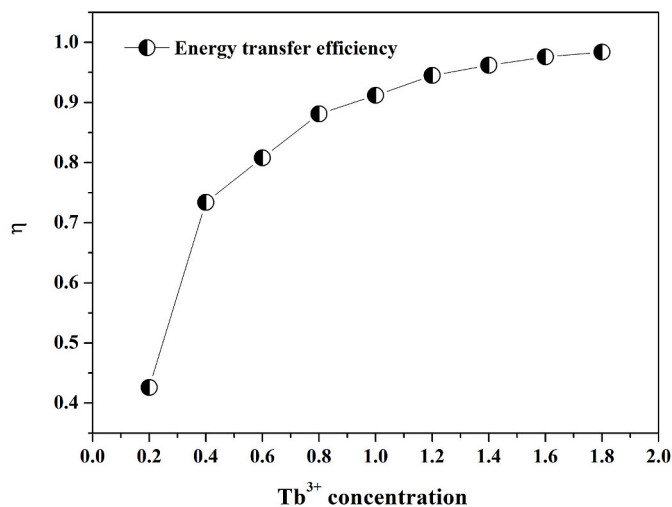


Fig. 6. Energy transfer efficiency of SGBO: 0.09Ce³⁺, yTb³⁺ phosphor.

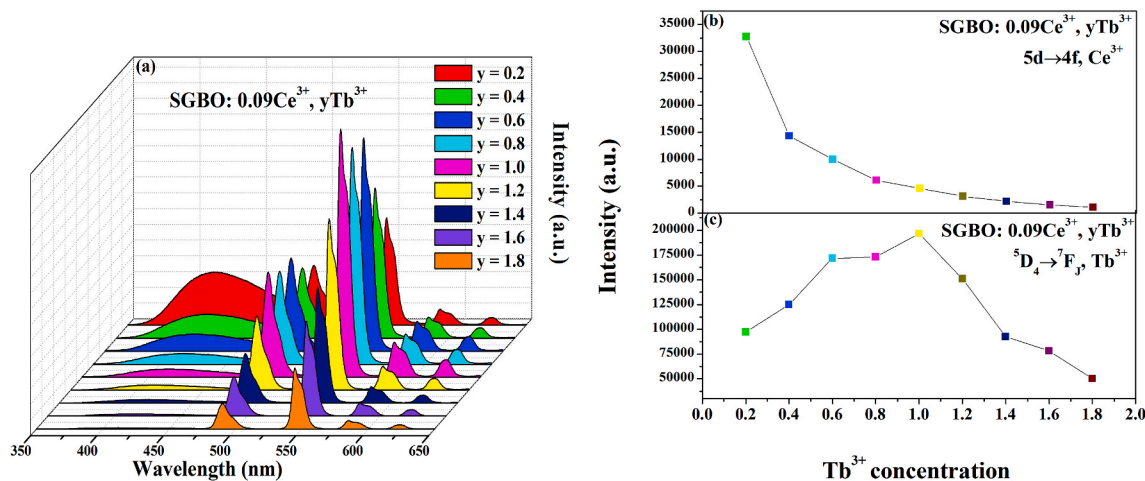


Fig. 5. (a) Spectra of SGBO: 0.09Ce³⁺, yTb³⁺ phosphors under 337 nm excitation. (b) Ce³⁺ ions and (c) Tb³⁺ ions emission intensity dependence.

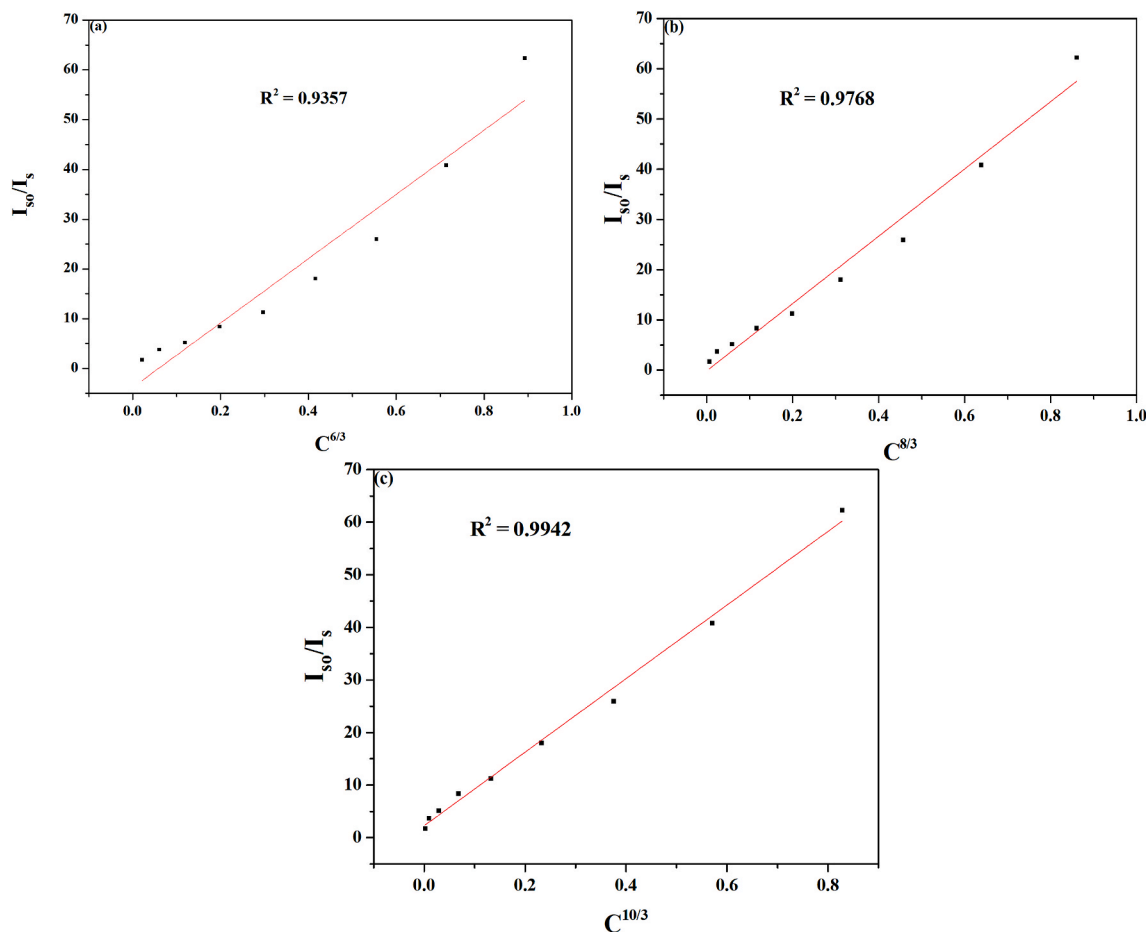


Fig. 7. Relationship diagram between I_{30}/I_s and (a) $C^{6/3}$, (b) $C^{8/3}$, (c) $C^{10/3}$.

3. Results and discussion

3.1. Phase identification

The XRD patterns of SGBO: 0.04Ce³⁺, SGBO: 0.09Ce³⁺, SGBO: 1.0 Tb³⁺ and SGBO: 0.09Ce³⁺, 1.0 Tb³⁺ phosphors were presented in Fig. 1. All of the diffraction peaks matched well with the standard card PDF # 00-058-0627, which was reported to crystallize in an orthorhombic crystal system with space group of Pmmm (47). Unit cell parameters $a = 7.4226 \text{ \AA}$, $b = 16.0624 \text{ \AA}$, $c = 8.7589 \text{ \AA}$, $\alpha = \beta = \gamma = 90^\circ$ and $V = 1044.28 \text{ \AA}^3$ [32]. There were no impurity peaks in the experimental range, which indicated that doping of Ce³⁺ ions and Tb³⁺ ions did not cause significant changes to the host structure. The radius of Ce³⁺ ions (1.034 Å) and Tb³⁺ ions (0.923 Å) were similar to the radius of Gd³⁺ ions (0.938 Å), therefore Ce³⁺ and Tb³⁺ ions replaced the position of Gd³⁺ sites in SGBO host.

3.2. Photoluminescence properties of SGBO: xCe³⁺ phosphors

Fig. 2(a) and (b) presented the emission spectra and excitation spectra of SGBO: xCe³⁺ ($x = 0.01, 0.02, 0.03, 0.04, 0.05, 0.075, 0.1, 0.15, 0.2$). Under the 342 nm excitation, SGBO: xCe³⁺ showed bright blue luminescence, and the broad emission bands extending from 350 nm to 600 nm were ascribed to the parity-allowed $5d \rightarrow 4f$ transitions of Ce³⁺ ions. When monitored at 424 nm emission, Ce³⁺ ions showed broad excitation bands ranged from 200 to 400 nm, which were attributed to the parity-allowed $4f \rightarrow 5d$ transition of Ce³⁺ ions [33,34]. At around 273 nm, all samples had a sharp peak, except SGBO: 0.2Ce³⁺ sample, which were ascribed to the $^8S_{7/2} \rightarrow ^6I_{13/2}$ transitions of Gd³⁺ ions. The

intensity of $^8S_{7/2} \rightarrow ^6I_{13/2}$ transitions decreased with the increasing of Ce³⁺ ions, and disappeared finally. It indicated that the excitation energy absorbed by Gd³⁺ ions decreased with the concentration increase of Ce³⁺ ions, and the energy transfer from Gd³⁺ ions to Ce³⁺ ions became weaker.

Fig. 2(c) showed the integral luminescence intensity of the SGBO: xCe³⁺ ($x = 0.01, 0.02, 0.03, 0.04, 0.05, 0.075, 0.1, 0.15, 0.2$) under 342 nm excitation. The luminescence intensity of SGBO: xCe³⁺ phosphors increased first ($x = 0.01-0.03$) and then decreased gradually ($x = 0.05-0.15$) with increasing Ce³⁺ ions concentrations. The optimum doping concentration of Ce³⁺ ions was $x = 0.04$. The luminescence intensity decreased greatly when the Ce³⁺ concentrations $x = 0.2$. This phenomenon was due to concentrations quenching.

Fig. 2(d) showed the emission spectrum of the SGBO: 0.04Ce³⁺ under the 342 nm excitation. The emission spectrum was analyzed by Gaussian fitting. The asymmetric Ce³⁺ emission band could be divided into two Gaussian bands centered at $24,570 \text{ cm}^{-1}$ (about 407 nm) and $22,717 \text{ cm}^{-1}$ (about 440 nm), which were attributed to the transitions from lowest 5d excited state to the $^2F_{5/2}$ and $^2F_{7/2}$ ground states of Ce³⁺ ions. The energy difference between these two bands was about 1853 cm^{-1} , which was close to the energy difference between the two sub-levels $^2F_{5/2}$ and $^2F_{7/2}$ ($\sim 2000 \text{ cm}^{-1}$) decomposed by the Ce³⁺ ions [35,36].

3.3. Photoluminescence properties of SGBO: xTb³⁺ phosphors

Fig. 3(a) presented the emission spectra of SGBO: xTb³⁺ ($x = 0.05, 0.1, 0.25, 0.5, 0.75, 1.0, 1.25, 1.5$) phosphors. Under 240 nm excitation, the emission spectra of SGBO: xTb³⁺ samples peaked at 490 nm, 544 nm, 585 nm, 623 nm, which were originated from the $^5D_4 \rightarrow ^7F_6$, $^5D_4 \rightarrow ^7F_5$,

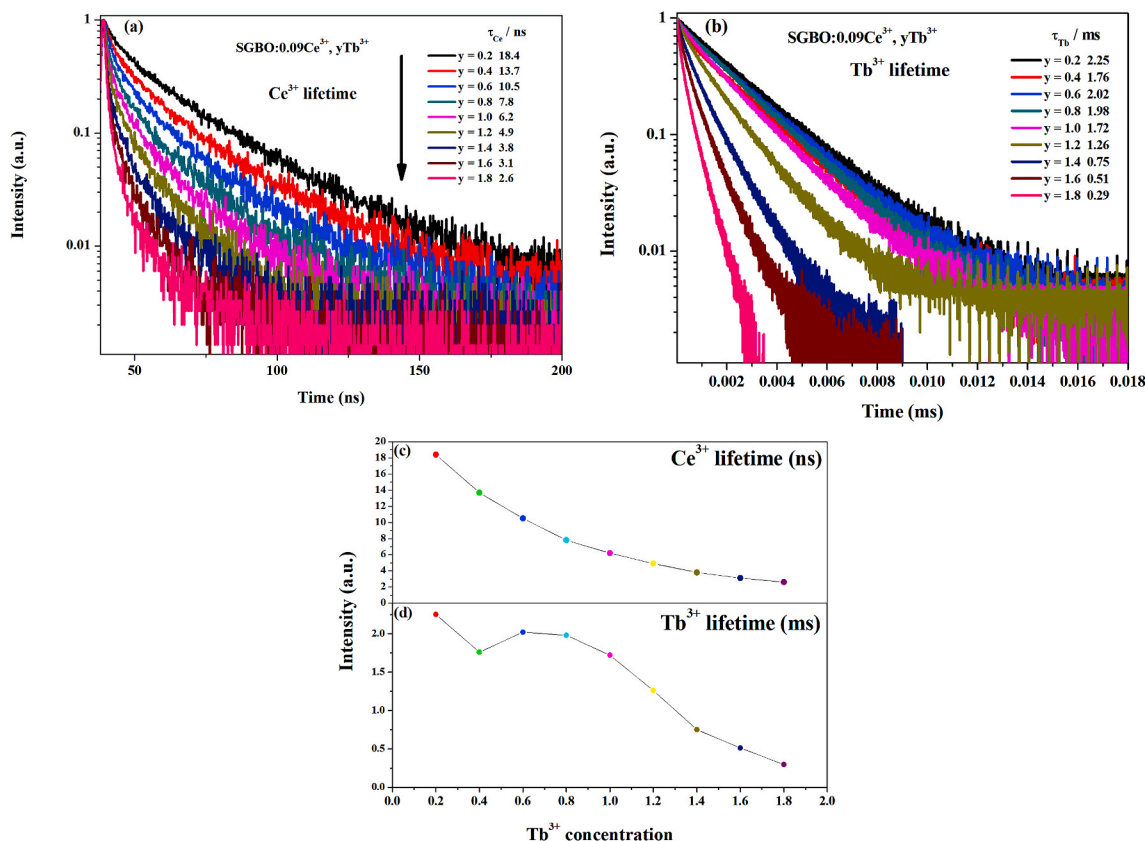


Fig. 8. (a) The decay curve of Ce³⁺ excitation at 337 nm when monitored under 415 nm. (b) The decay curve of Tb³⁺ excitation at 355 nm when monitored at 544 nm. (c) Ce³⁺ ions and (d) Tb³⁺ ions lifetime dependence with Tb³⁺ ions concentration.

Table 1
Ce³⁺ and Tb³⁺ ions lifetime dependence with Tb³⁺ ions concentration.

Tb ³⁺ concentration	Ce ³⁺ lifetime (ns)	Tb ³⁺ lifetime (ms)
0.2	18.4	2.25
0.4	13.7	1.76
0.6	10.5	2.02
0.8	7.8	1.98
1.0	6.2	1.72
1.2	4.9	1.26
1.4	3.8	0.75
1.6	3.1	0.51
1.8	2.6	0.29

⁵D₄ → ⁷F₄, ⁵D₄ → ⁷F₃ transition of Tb³⁺ ions, respectively [37,38]. Fig. 3 (b) presented the excitation spectra of SGBO: xTb³⁺ (x = 0.05, 0.1, 0.25, 0.5, 0.75, 1.0, 1.25, 1.5) phosphors. The excitation spectra were obtained by monitoring the 544 nm emission. The phosphor exhibited a broad excitation in the range of 200 nm–300 nm, which was attributed to the 4f → 5d transition of Tb³⁺ ions. Two sharp peaks were observed at around 273 nm and 317 nm, which were ascribed to the ⁸S_{7/2} → ⁶I_{13/2} and ⁸S_{7/2} → ⁶P_{7/2} transitions of Gd³⁺ ions. This indicated the occurrence of energy transfer from Gd³⁺ ions to Tb³⁺ ions [39,40]. Also, several sharp excitation peaks were obtained in the range of 300 nm–500 nm, which could be attributed to the parity-forbidden 4f → 4f transition of Tb³⁺ ions.

3.4. Photoluminescence and energy transfer of SGBO: Ce³⁺, Tb³⁺ properties

Fig. 4(a) showed two different excitation bands appeared in the excitation spectra at around 284 nm and 342 nm, which monitored at

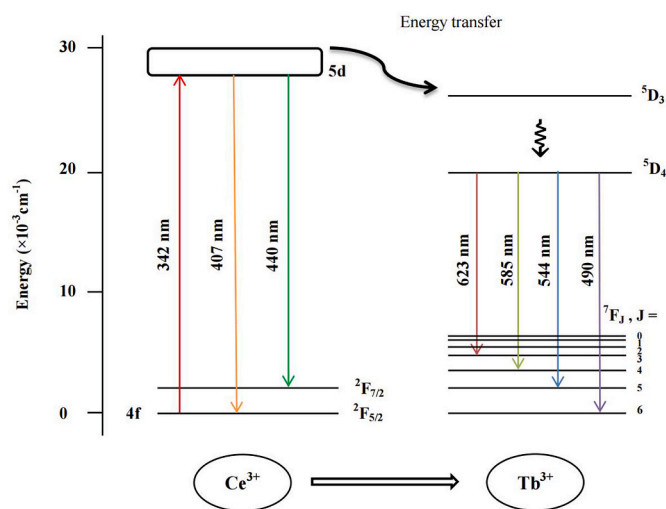


Fig. 9. Energy levels transition of Ce³⁺ and Tb³⁺ in SGBO.

424 nm. And these bands originated from the 4f → 5d transition of Ce³⁺ ions, and the strongest excitation band was at around 342 nm [41]. The photoluminescence spectrum exhibited a broad band peaked at 424 nm excited by near ultraviolet 342 nm, which was assigned to the transition from the lowest 5d state to the 4f ground state of Ce³⁺.

The emission and excitation spectra of SGBO: 1.0 Tb³⁺ sample was presented in Fig. 4(b). The excitation wavelength was 273 nm. It could be clearly seen that the emission spectrum included a series of emission peaks in the range of 450 nm–650 nm. The emission peaked at 490 nm, 544 nm, 584 nm, 623 nm, which were attributed to the ⁵D₄ → ⁷F₆, ⁵D₄ →

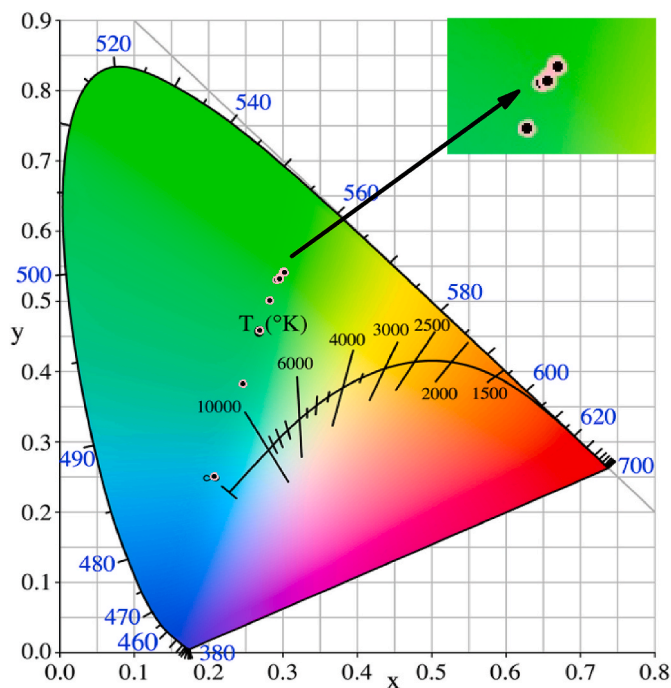


Fig. 10. The CIE 1931 diagram of SGBO: 0.09Ce³⁺, yTb³⁺ under 337 nm excitation.

Table 2

The CIE in SGBO: 0.09Ce³⁺, yTb³⁺ under 337 nm excitation.

sample	CIE (x, y)
SGBO: 0.09Ce ³⁺ , 0.2Tb ³⁺	(0.21, 0.25)
SGBO: 0.09Ce ³⁺ , 0.4Tb ³⁺	(0.25, 0.38)
SGBO: 0.09Ce ³⁺ , 0.6Tb ³⁺	(0.27, 0.46)
SGBO: 0.09Ce ³⁺ , 0.8Tb ³⁺	(0.28, 0.50)
SGBO: 0.09Ce ³⁺ , 1.0Tb ³⁺	(0.29, 0.53)
SGBO: 0.09Ce ³⁺ , 1.2Tb ³⁺	(0.30, 0.53)
SGBO: 0.09Ce ³⁺ , 1.4Tb ³⁺	(0.30, 0.53)
SGBO: 0.09Ce ³⁺ , 1.6Tb ³⁺	(0.30, 0.54)
SGBO: 0.09Ce ³⁺ , 1.8Tb ³⁺	(0.30, 0.54)

⁷F₅, ⁵D₄ → ⁷F₄, ⁵D₄ → ⁷F₃ transition of Tb³⁺ ions [42]. When monitored at 544 nm, the excitation spectrum consists of a broad band and a series of sharp peaks. The broad excitation band at around 240 nm was attributed to the 4f⁸ → 4f⁷5d transition of Tb³⁺ ions. Two sharp peaks were observed at around 273 nm and 317 nm, which were attributed to the transitions of Gd³⁺ ions [43]. The excitation peaked in the wavelength range of 300–520 nm were attributed to the 4f → 4f electronic transition of Tb³⁺ ions.

It was obvious that the emission spectrum of Ce³⁺ ions overlap with the excitation band of Tb³⁺ ions. It indicated that the possibility of energy transfer from Ce³⁺ to Tb³⁺ according to Dexter's theory [44,45]. As shown in Fig. 4(c), when monitored at 545 nm, SGBO: 0.09Ce³⁺, 1.0 Tb³⁺ excitation band showed the characteristic of 4f → 5d transition of Ce³⁺ ions. At the same time, upon 337 nm, not only Ce³⁺ ions emission but also strong Tb³⁺ ions emission appeared in the photoluminescence spectrum.

The photoluminescence intensity of the SGBO: xCe³⁺, 1.0 Tb³⁺ phosphor was measured, the SGBO: 0.09Ce³⁺, 1.0 Tb³⁺ was brightest, so the concentration of Ce³⁺ was fixed at x = 0.09 in the next experiment. The photoluminescence spectra of SGBO: 0.09Ce³⁺, yTb³⁺ (y = 0.2, 0.4, 0.6, 0.8, 1.0, 1.2, 1.4, 1.6, 1.8) phosphors under 337 nm excitation were shown in Fig. 5(a). Fig. 5(b) showed the emission intensity of Ce³⁺ ions upon 337 nm excitation. It was clearly found that the blue emission intensity of Ce³⁺ ions decreased with the Tb³⁺ ions doping

concentrations increased. Fig. 5(c) presented the ⁵D₄ → ⁷F_J (J = 6, 5, 4, 3) emission intensity of Tb³⁺ ions, which was increased first and then decreased with the increasing in Tb³⁺ ions concentrations, Tb³⁺ ions optimum doping concentrations was y = 1.0.

Energy transfer efficiency was calculated by the following formula:

$$\eta = 1 - \frac{I_s}{I_{so}} \quad (1)$$

where η represented energy transfer efficiency between Ce³⁺ ions and Tb³⁺ ions, where I_s was the emission intensity of Ce³⁺ with co-doped Tb³⁺ ions, I_{so} was the emission intensity of Ce³⁺ in the absence of Tb³⁺ ions [46]. Energy transfer efficiency of SGBO: 0.09Ce³⁺, yTb³⁺ phosphor were plotted in Fig. 6. With the increasing in concentrations of Tb³⁺ ions, energy transfer efficiency gradually improved. When the Tb³⁺ ions concentration was y = 1.8, the energy transfer efficiency reached 98.37%.

There were two main mechanisms of energy transfer: electric multipole interaction and exchange interaction. Electric multipole interaction included dipole-dipole, dipole-quadrupole and quadrupole-quadrupole interactions. Electric multipole interaction and exchange interaction were determined mainly by the critical distance (R_c) between activator (Tb³⁺) and the sensitizer (Ce³⁺). General, while $R_c \leq 5$ Å, energy transfer was dominated by exchange interaction, when $R_c > 5$ Å, the energy transfer was mainly attributed to the electric multipole interaction.

The critical distance (R_c) could be obtained by the following formula:

$$R_c = 2 \left(\frac{3V}{4\pi CN} \right)^{1/3} \quad (2)$$

where R_c was critical distance, V was the volume of the unit cell ($V = 1044$ Å³), N was the number of sites in a unit cell that could be occupied by the activator ($N = 8$), C was the total concentrations of activator (Tb³⁺) and the sensitizer (Ce³⁺) ($C = 0.545$) [47,48]. R_c was calculated to be 7.7 Å. Therefore, the main mechanism of energy transfer of Ce³⁺ to Tb³⁺ was electric multipole interaction.

According to Dexter energy transfer mechanism and Reisfeld's approximation, the energy transfer mechanism of the electric multipole interaction could be further determined by the following formula:

$$\frac{\eta_{so}}{\eta_s} \approx \frac{I_{so}}{I_s} \propto C^n \quad (3)$$

where η_{so} and η_s represented quantum efficiency. I_{so} and I_s was the luminescence intensities of Ce³⁺ in the presence and absence of ions. We calculated it with I_{so} and I_s . The number n was equal to 6, 8 and 10, corresponding to dipole-dipole, dipole-quadrupole and quadrupole-quadrupole interactions [49]. Fig. 7 showed the relationship between C^n and I_{so}/I_s . When n was equal to 10, the linear fit was best. The consequences distinctly showed that the energy transfer between Tb³⁺ and Ce³⁺ in the SGBO host was due to the quadrupole-quadrupole interaction.

Fig. 8(a) and (b) showed the decay curves of Ce³⁺ ions and Tb³⁺ ions. The lifetime of the samples could be obtained by calculating the curve areas. Fig. 8(c) and (d) showed the lifetime of Ce³⁺ ions and Tb³⁺ ions. Table 1 showed the Ce³⁺ and Tb³⁺ ions lifetime dependence with Tb³⁺ ions concentration. With the increasing of doping concentrations of Tb³⁺ ions, the decay times of Ce³⁺ ions and Tb³⁺ ions decreased. If the sensitizer (Ce³⁺) had energy transfer functional on the activator (Tb³⁺). The decay times decreased with increasing the activator doping concentration, which could explain the existence of energy transfer from Ce³⁺ ions to Tb³⁺ ions [50–52]. When the concentration of Tb³⁺ was more than x = 1.2, the lifetime of Tb³⁺ ions became shorter and shorter, which was due to concentrations quenching.

Energy transfer level diagram of Ce³⁺ ions and Tb³⁺ ions in SGBO was shown in Fig. 9. Ce³⁺ ions were excited from ground state to 5d

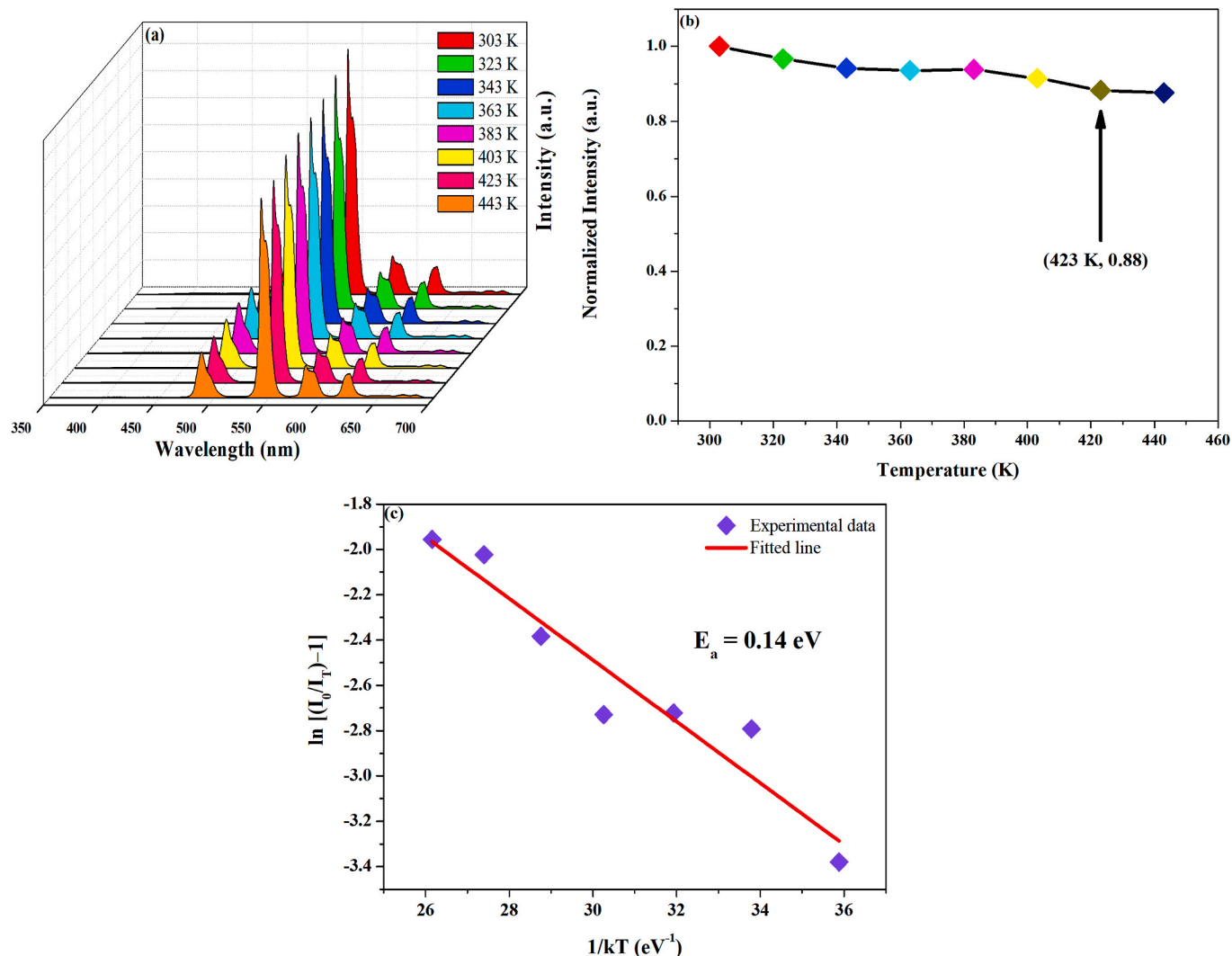


Fig. 11. (a) Temperature dependent emission spectra of SGBO: 0.09Ce³⁺, 1.0 Tb³⁺ green phosphor ($\lambda_{ex} = 325$ nm). (b) The relative emission intensity with different temperatures. (c) Plot of $\ln[(I_0/I_T)-1]$ versus $1/kT$ for SGBO: 0.09Ce³⁺, 1.0 Tb³⁺ phosphor.

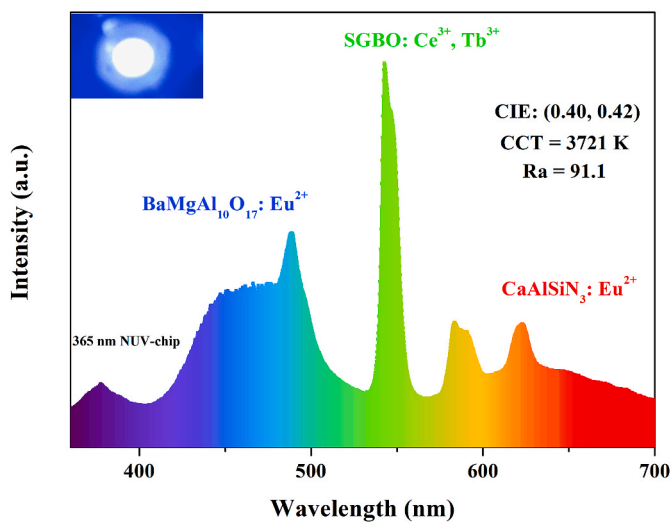


Fig. 12. The emission spectrum of a 365 nm near ultraviolet chip based white LED using BaMgAl₁₀O₁₇: Eu²⁺ (blue), SGBO: 0.09Ce³⁺, 1.0 Tb³⁺ (green), and CaAlSiN₃: Eu²⁺ (red) phosphors. Inset showed the photo of the white LED package.

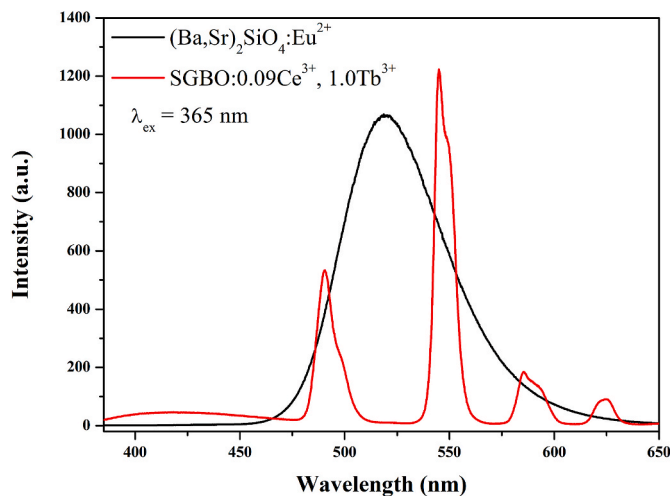


Fig. 13. Emission spectra of SGBO: 0.09Ce³⁺, 1.0 Tb³⁺ phosphor and commercial (Ba, Sr)₂SiO₄: Eu²⁺ phosphor under 365 nm excitation.

Table 3

The IQE and EQE of SGBO: 0.09Ce³⁺, SGBO: 0.09Ce³⁺, 1.0 Tb³⁺, (Ba, Sr)₂SiO₄: Eu²⁺ phosphor. ($\lambda_{\text{ex}} = 345 \text{ nm}$).

Sample	IQE	EQE
SGBO: 0.09Ce ³⁺	32.2%	26.6%
SGBO: 0.09Ce ³⁺ , 1.0 Tb ³⁺	57.9%	46.0%
(Ba, Sr) ₂ SiO ₄ : Eu ²⁺	74.6%	64.3%

excited state. One part of the excited Ce³⁺ ions returned to the ground states, another part of the excited Ce³⁺ ions transferred energy to the excited state (⁵D₃) of Tb³⁺ ions. The ⁵D₃ state of Tb³⁺ ions relaxed to ⁵D₄ state. Finally, Tb³⁺ ions gave rise to green emission.

Fig. 10 presented the position of each concentration samples in CIE 1931. The CIE coordinates of SGBO: 0.09Ce³⁺, yTb³⁺ (y = 0.2, 0.4, 0.6, 0.8, 1.0, 1.2, 1.4, 1.6, 1.8) excited by 337 nm were displayed in Table 2. From the CIE coordinates of the samples, with the increasing of Tb³⁺ ions concentration, the samples could be modulated from white (0.21, 0.25) to green (0.30, 0.54). The photoluminescence spectra were mainly determined by the emission of Tb³⁺ ions, and showed green light.

3.5. Thermal stability and activation energy

Thermal stability is an important parameter in luminescent materials to assess whether the phosphors are suitable for LEDs. The temperature dependent emission spectra of SGBO: 0.09Ce³⁺, 1.0 Tb³⁺ sample from 303 K to 443 K were presented in Fig. 11(a). It was clearly seen that with the temperature increasing the emission intensity of all transitions decreased due to the thermal quenching effect [35,53,54]. Fig. 11(b) showed the emission intensity dependence on temperature. At 443 K, the emission intensity reached 88% of the initial value. The SGBO: 0.09Ce³⁺, 1.0 Tb³⁺ phosphor exhibited relatively high thermal stability favorable for LEDs application. We also determined the activation energy of SGBO: 0.09Ce³⁺, 1.0 Tb³⁺ green phosphor by following Arrhenius equation [55]:

$$I_T = I_0 \left[1 + C \exp\left(-\frac{E_a}{kT}\right) \right]^{-1} \quad (4)$$

where I_T was the emission intensity at test temperature (T); I_0 was the emission intensity at 303 K; C was a constant; E_a was the activation energy for thermal quenching; k was the Boltzmann constant ($8.62 \times 10^{-5} \text{ eV/K}$) and T was the temperature in K. Fig. 11 (c) showed the plot of $\ln[(I_0/I_T)-1]$ versus $1/kT$ for SGBO: 0.09Ce³⁺, 1.0 Tb³⁺ green phosphor. The slope of the fitted line was about 0.14. Therefore, the activation energy of SGBO: 0.09Ce³⁺, 1.0 Tb³⁺ green phosphor was calculated, and it was 0.14 eV [56,57].

3.6. Application in white LED

A white LED was fabricated by using a 365 nm near-ultraviolet LED chip combined with BaMgAl₁₀O₁₇: Eu²⁺ (blue), SGBO: 0.09Ce³⁺, 1.0 Tb³⁺ (green), and CaAlSiN₃: Eu²⁺ (red) phosphors, the emission spectrum was shown in Fig. 12. The color coordinates (CIE), correlated color temperature (CCT) and color rendering index (Ra) of LED were determined to be (0.40, 0.42), 3721 K and 91.1, respectively. All the results showed that SGBO: Ce³⁺, Tb³⁺ has the potential to be used as a green phosphor for near ultraviolet white light LEDs.

Fig. 13 showed the emission intensity of SGBO: 0.09Ce³⁺, 1.0 Tb³⁺ phosphor and commercial (Ba, Sr)₂SiO₄: Eu²⁺ phosphor under 365 nm excitation. Although the integrated luminescence intensity of SGBO: 0.09Ce³⁺, 1.0 Tb³⁺ phosphor was about 40% of (Ba, Sr)₂SiO₄: Eu²⁺ phosphor, the 545 nm peak emission intensity of SGBO: 0.09Ce³⁺, 1.0 Tb³⁺ phosphor was higher than the commercial (Ba, Sr)₂SiO₄: Eu²⁺ phosphor. Table 3 presented the IQEs and EQEs of SGBO: 0.09Ce³⁺ and SGBO: 0.09Ce³⁺, 1.0 Tb³⁺ phosphor under 345 nm excitation, IQEs were

about 32.2% and 57.9%, EQEs were about 26.6% and 46.0%. The IQE of SGBO: 0.09Ce³⁺, 1.0 Tb³⁺ phosphor has reached 74.3% of commercial (Ba, Sr)₂SiO₄: Eu²⁺ phosphor.

4. Conclusions

In summary, a series of green color tunable SGBO: Ce³⁺, SGBO: Tb³⁺, SGBO: Ce³⁺, Tb³⁺ were successfully synthesized through conventional high temperature solid state reaction method. The XRD results indicated that SGBO: Ce³⁺, SGBO: Tb³⁺ and SGBO: Ce³⁺, Tb³⁺ phosphors were pure phase. Fluorescence spectra showed the optimum concentration of SGBO: xCe³⁺ was x = 0.04, the optimum concentration of SGBO: xTb³⁺ was x = 1.0. With the concentrations of Tb³⁺ ions increasing, the efficiency from Ce³⁺ ions to Tb³⁺ ions energy transfer increased. The maximum energy transfer efficiency reached 98.37%. By measuring the fluorescence lifetime decay curves of Ce³⁺ and Tb³⁺, it was further proved that the energy of Ce³⁺ ions were transferred to Tb³⁺ ions, and the energy transfer caused by quadrupole-quadrupole interaction. With the concentrations of Tb³⁺ ions increasing its CIE modulated from white (0.21, 0.25) to green (0.30, 0.54). When temperature reached 423 K, the luminescence intensity reached 88% of the initial value, indicating that SGBO: Ce³⁺, Tb³⁺ have excellent thermal stability. A white LED was fabricated by using a 365 nm near ultraviolet LED chip combined with BaMgAl₁₀O₁₇: Eu²⁺ blue phosphor, SGBO: 0.09Ce³⁺, 1.0 Tb³⁺ green phosphor and CaAlSiN₃: Eu²⁺ red phosphor. The CIE was (0.40, 0.42); CCT was 3721 K; and Ra of LED was 91.1. The IQEs of SGBO: 0.09Ce³⁺ and SGBO: 0.09Ce³⁺, 1.0 Tb³⁺ phosphor under 345 nm excitation were about 32.2% and 57.9%. These results indicated that SGBO: Ce³⁺, Tb³⁺ could be as a potential green LED phosphor.

Author statement

Xiaoxuan Fan: Investigation, data sorting, software, writing-manuscript preparation. Xiaoyuan Sun: Conceptualization, funding acquisition, supervision, writing-review and editing. Chunmiao Liu: Investigation. Wanlu Tian: Investigation. Min Li: Investigation. Yongshi Luo: Methodology, formal analysis. Chunlei Wu: Methodology, funding acquisition.

Declaration of competing interest

The authors declare that they have no known competing financial interests or personal relationships that could have appeared to influence the work reported in this paper.

Acknowledgements

This work is financially supported by the Technology Development Plan of Jilin Province (Grant No. YDZJ202101ZYTS176), the Natural Science Foundation of Changchun Normal University, the Fundamental Research Funds for Heilongjiang Provincial Universities (No. 1355MSYYB008), and the Scientific Research Project of Mudanjiang Normal University (No. YB202004).

References

- [1] T. Yang, H. Huang, C. Sun, B. Glorieux, X. Lee, Y. Yu, T. Chung, Noncontact and instant detection of phosphor temperature in phosphor-converted white LEDs, *Nature* 8 (2018) 1–10.
- [2] X. Huang, Red phosphor converts white LEDs, *Nat. Photonics* 8 (2014) 748–749.
- [3] Y. Ahn, K. Kim, G. Anoop, G. Kim, J. Yoo, Design of highly efficient phosphor-converted white light-emitting diodes with color rendering indices ($R_1 - R_{15}$) ≥ 95 for artificial lighting, *Sci. Rep.* 9 (2019) 1–10.
- [4] J. Qiao, G. Zhou, Y. Zhou, Q. Zhang, Z. Xia, Divalent europium-doped near-infrared-emitting phosphor for light-emitting diodes, *Nat. Commun.* 10 (2019) 1–7.
- [5] X. Zhu, X. Guo, J. Zhang, J. Liu, F. Jiang, Phosphor-free, color-mixed, and efficient illuminant: multi-chip packaged LEDs for optimizing blue light hazard and non-visual biological effects, *Opt Laser. Eng.* 134 (2020) 106174.

- [6] M.A. Alim, M.Z. Abdullah, M.S. Abdul Aziz, R. Kamarudin, Die attachment, wire bonding, and encapsulation process in LED packaging: a review, *Sens. Actuators, A* 329 (2021) 112817.
- [7] E. Ozuturk, A system and a method to measure the junction temperature of LEDs, *Optik* 235 (2021) 166655.
- [8] X. Jiang, C. Zheng, C. Mo, X. Wang, J. Zhang, Z. Quan, J. Liu, F. Jiang, Interface modification of two-step grown InGaN/GaN superlattices preparing layers for InGaN-based green LED on silicon substrate, *Superlattice. Microst.* 126 (2019) 120–124.
- [9] H. Althib, Effect of quantum barrier width and quantum resonant tunneling through InGaN/GaN parabolic quantum well-LED structure on LED efficiency, *Results Phys.* 22 (2021) 103943.
- [10] R. Zhang, J.F. Sun, An efficient perovskite-type $\text{Rb}_2\text{CaPO}_4\text{:Eu}^{2+}$ phosphor with high brightness towards closing the cyan gap, *J. Alloys Compd.* 872 (2021) 159698.
- [11] W. Nemitz, P. Fulmek, J. Nocolis, F. Reil, F.P. Wenzl, On the determination of the temperature distribution within the color conversion elements of phosphor converted LEDs, *Sci. Rep.* 7 (2017) 1–10.
- [12] P. Singh, C.M. Tan, Degradation physics of high power LEDs in outdoor environment and the role of phosphor in the degradation process, *Sci. Rep.* 6 (2016) 1–13.
- [13] T. Hu, L. Ning, Y. Gao, J. Qiao, E. Song, Z. Chen, Y. Zhou, J. Wang, M.S. Molokeev, X. Ke, Z. Xia, Q. Zhang, Glass crystallization making red phosphor for high-power warm white lighting, *Light Sci. Appl.* 10 (2021) 1–12.
- [14] K. Rajfur, P. Gluchowski, Design of the persistent luminescence colour of a novel $\text{Gd}_{3-x}\text{Tb}_x\text{Ga}_3\text{Al}_2\text{O}_{12}$ phosphor: synthesis methods, spectroscopic properties and mechanism, *Dalton Trans.* 50 (2021) 4830–4839.
- [15] M.M. Yerpude, G.B. Nair, S.J. Dhoble, S.H. Bagade, H.C. Swart, Sensitization of Tb^{3+} and Dy^{3+} emission in $\text{Li}_4\text{Ca}(\text{BO}_3)_2$ via energy transfer from Ce^{3+} and study of energy transfer mechanism, *Optik* 218 (2020) 164977.
- [16] Y. Zhou, Y. Li, H. Wu, X. Li, M. Guo, High temperature persistent luminescence in Tb^{3+} doped $\text{CaSr}_2\text{Al}_2\text{O}_6$ phosphor, *Optik* 242 (2021) 167103.
- [17] P. Pei, P.D. Mu, B. Wang, X. Miao, C. Zhang, W. Liu, An advanced color tunable persistent luminescent $\text{NaCa}_2\text{GeO}_4\text{:F:Tb}^{3+}$ phosphor for multicolor anti-counterfeiting, *Dalton Trans.* 50 (2021) 3193–3200.
- [18] M. Qu, X. Zhang, X. Mi, H. Sun, Q. Liu, Z. Bai, Luminescence color tuning of Ce^{3+} and Tb^{3+} co-doped $\text{Ca}_2\text{Yzr}_2\text{Al}_3\text{O}_{12}$ phosphors with high color rendering index via energy transfer, *J. Lumin.* 228 (2020) 117557.
- [19] X. Huang, J. Liang, S. Rtimi, B. Devalumar, Z. Zhang, Ultra-high color rendering warm-white light-emitting diodes based on an efficient green-emitting garnet phosphor for solid-state lighting, *Chem. Eng. J.* 405 (2021) 126950.
- [20] J. Liang, B. Devakumar, L. Sun, S. Wang, Q. Sun, X. Huang, Full-visible-spectrum lighting enabled by an excellent cyan-emitting garnet phosphor, *J. Mater. Chem. C* 8 (2020) 4934–4943.
- [21] N. Ma, W. Li, B. Devakumar, Z. Zhang, X. Huang, Utilizing energy transfer strategy to produce efficient green luminescence in $\text{Ca}_2\text{LuHf}_2\text{Al}_3\text{O}_{12}$: Ce^{3+} , Tb^{3+} garnet phosphors for high-quality near-UV-pumped warm-white LEDs, *J. Colloid Interface Sci.* 601 (2021) 365–377.
- [22] Y. Zhao, S. Wang, Y. Han, J. Zhang, C. Liu, X. Hu, Z. Zhang, L. Wang, Luminescence properties and energy transfer in Ce^{3+} and Tb^{3+} co-doped $\text{Sr}_5(\text{PO}_4)_2\text{SiO}_4$ phosphor, *J. Lumin.* 223 (2020) 117253.
- [23] S. Wang, B. Devakumar, Q. Sun, J. Liang, L. Sun, X. Huang, Highly efficient near-UV-excitable $\text{Ca}_2\text{YHf}_2\text{Al}_3\text{O}_{12}$: Ce^{3+} , Tb^{3+} green-emitting garnet phosphors with potential application in high color rendering warm-white LEDs, *J. Mater. Chem. C* 8 (2020) 4408–4420.
- [24] F. Junqin, J. Cao, Z. Li, Z. Li, J. Li, J. Lin, W. Li, Z. Mu, F. Wu, The luminescence properties, energy transfer mechanism of the color tunable and high quantum efficiency $\text{LaAl}_{2.03}\text{B}_4\text{O}_{10.54}$: Ce^{3+} , Tb^{3+} phosphors, *Ceram. Int.* 45 (2019) 20316–20322.
- [25] Y. Xiao, Z. Hao, L. Zhang, X. Zhang, G.H. Pan, H. Wu, H. Wu, Y. Luo, J. Zhang, An efficient green phosphor of Ce^{3+} and Tb^{3+} -codoped $\text{Ba}_2\text{Lu}_3\text{B}_5\text{O}_{17}$ and a model for elucidating the high thermal stability of the green emission, *J. Mater. Chem. C* 6 (2018) 5984–5991.
- [26] P. Wu, X. Tong, Y. Xu, J. Han, H.J. Seo, X. Zhang, Investigation of site occupancy and photoluminescence of Ce^{3+} in cubic borate $\text{Ba}_3\text{Y}_2(\text{B}_2\text{O}_5)_3$ and $\text{Ce}^{3+} > \text{Tb}^{3+}$ energy transfer behavior, *Opt. Mater.* 91 (2019) 246–252.
- [27] H. Li, Y. Liang, S. Liu, W. Zhang, Y. Bi, Y. Gong, Y. Chen, W. Lei, Highly efficient green-emitting phosphor $\text{Sr}_4\text{Al}_{14}\text{O}_{25}$: Ce, Tb with low thermal quenching and wide color gamut upon UV-light excitation for backlighting display applications, *J. Mater. Chem. C* 9 (2021) 2569–2581.
- [28] M. Xin, D. Tu, H. Zhu, W. Luo, Z. Liu, P. Huang, R. Li, Y. Cao, X. Chen, Single-composition white-emitting NaSrBO_3 : Ce^{3+} , Sm^{3+} , Tb^{3+} phosphors for NUV light-emitting diodes, *J. Mater. Chem. C* 3 (2015) 7286–7293.
- [29] D. Geng, G. Li, M. Shang, D. Yang, Y. Zhang, Z. Cheng, J. Lin, Color tuning via energy transfer in $\text{Sr}_3\text{In}(\text{PO}_4)_3$: $\text{Ce}^{3+}/\text{Tb}^{3+}/\text{Mn}^{2+}$ phosphors, *J. Mater. Chem.* 22 (2012) 14262–14271.
- [30] X. Sun, W. Gao, T. Yang, R. Cong, Sol-gel syntheses, luminescence, and energy transfer properties of $\alpha\text{-GdB}_5\text{O}_9$: $\text{Ce}^{3+}/\text{Tb}^{3+}$ phosphors, *Dalton Trans.* 44 (2015) 2276–2284.
- [31] A. Shyichuk, S. Lis, Green-emitting nanoscaled borate phosphors $\text{Sr}_3\text{RE}(\text{BO}_3)_4$: Tb^{3+} , *Mater. Chem. Phys.* 140 (2013) 447–452.
- [32] S. He, F. Yuan, L. Liu, Y. Huang, L. Zhang, Z. Lin, Crystal growth and spectroscopic characterization of Dy^{3+} : $\text{Sr}_3\text{Gd}_2(\text{BO}_3)_4$ - A potential yellow solid state laser material, *Opt. Mater.* 111 (2021) 110562.
- [33] W. Lei, Z. Luo, Y. He, S. Liu, P. Zhang, H. Liang, A. Lu, Preparation and broadband white emission of Ce^{3+} -doped transparent glass-ceramics containing ZnO nanocrystals for WLEDs applications, *J. Alloys Compd.* 875 (2021), 159979.
- [34] J. Li, Z. Ma, F. Wang, Z. Wang, Synthesis and mechanoluminescent properties of submicro-sized $\text{Y}_3\text{Al}_5\text{O}_{12}$: Ce^{3+} particles, *Chem. Phys. Lett.* 775 (2021) 138664.
- [35] S. Wang, B. Devakumar, Q. Sun, J. Liang, L. Sun, X. Huang, Efficient green-emitting $\text{Ca}_2\text{GdZr}_2\text{Al}_3\text{O}_{12}$: Ce^{3+} , Tb^{3+} phosphors for near-UV-pumped high-CRI warm-white LEDs, *J. Lumin.* 220 (2020) 117012.
- [36] L. Sun, B. Devakumar, J. Liang, S. Wang, Q. Sun, X. Huang, Highly efficient $\text{Ce}^{3+} \rightarrow \text{Tb}^{3+}$ energy transfer induced bright narrowband green emissions from garnet-type $\text{Ca}_2\text{YZr}_2(\text{AlO}_4)_3$: Ce^{3+} , Tb^{3+} phosphors for white LEDs with high color rendering index, *J. Mater. Chem. C* 7 (2019) 10471–10480.
- [37] L. Han, J. Liu, P. Liu, B. Li, X. Li, Y. Xu, Dual-emissive Eu^{3+} , Tb^{3+} co-doped $\text{Gd}_2(\text{MoO}_4)_3$ phosphor for optical thermometry application, *J. Phys. Chem. Solid.* 153 (2021) 110032.
- [38] Y. Li, Y. Zhou, X. Li, H. Wu, L. Zhao, W. Wang, Energy transfer and the anti-thermal quenching behavior of $\text{Sr}_8\text{MgCe}(\text{PO}_4)_7$: Tb^{3+} for temperature sensing, *Spectrochim. Acta A* 252 (2021) 119548.
- [39] B. Qian, Z. Wang, Y. Wang, Q. Zhao, X. Zhou, H. Zou, Y. Song, Y. Sheng, Comparative study on the morphology, growth mechanism and luminescence property of $\text{RE}_2\text{O}_3\text{S}$: Eu^{3+} (RE = Lu, Gd, Y) phosphors, *J. Alloys Compd.* 870 (2021) 159273.
- [40] R. Yun, J. He, L. Luo, X. Liu, Z. Nie, W. Zhao, H. Wen, Upconversion luminescence and temperature sensing properties in $\text{LiGd}(\text{WO}_4)_2$: Er^{3+} , Yb^{3+} , Nd^{3+} microparticles under 785 nm excitation, *Ceram. Int.* 47 (2021) 16062–16069.
- [41] H. Ding, Z. Liu, Y. Liu, P. Hu, P. Sun, Z. Luo, K. Chao, H. Jiang, J. Jiang, $\text{Gd}_3\text{Al}_3\text{Ga}_2\text{O}_{12}$: Ce, Mg²⁺ + transparent ceramic phosphors for high-power white LEDs/LDs, *Ceram. Int.* 47 (2020) 7918–7924.
- [42] V. Singh, S. Tamboli, S.J. Dhoble, H. Jeong, Ultraviolet, vacuum ultraviolet excited photoluminescence study of sol-gel derived CaAl_4O_7 : Tb^{3+} green emitting phosphor, *Optik* 213 (2020) 164375.
- [43] Q. He, Y. Zhang, Y. Yu, Y. Chen, M. Jin, E. Mei, X. Liang, L. Zhai, W. Xiang, Ultra-stable Gd^{3+} doped CsPbBr_2 nanocrystals red glass for high efficiency WLEDs, *Chem. Eng. J.* 411 (2021) 128530.
- [44] Y. Zhao, S. Wang, Y. Han, J. Zhang, C. Liu, X. Hu, Z. Zhang, L. Wang, Luminescence properties and energy transfer in Ce^{3+} and Tb^{3+} co-doped $\text{Sr}_5(\text{PO}_4)_2\text{SiO}_4$ phosphor, *J. Lumin.* 223 (2020) 117253.
- [45] Y. Li, Y. Yin, T. Wang, J. Wu, J. Zhang, S. Yu, M. Zhang, L. Zhao, W. Wang, Ultra-bright green-emitting phosphors with an internal quantum efficiency of over 90% for high-quality WLEDs, *Dalton Trans.* 50 (2021) 4159–4166.
- [46] F. Wang, H. Song, G. Pan, L. Fan, B. Dong, L. Liu, X. Bai, R. Qin, X. Ren, Z. Zheng, S. Lu, Luminescence properties of Ce^{3+} and Tb^{3+} ions codoped strontium borate phosphate phosphors, *J. Lumin.* 138 (2008) 2013–2018.
- [47] P. Liang, Co-existence phenomenon of $\text{Ce}^{3+}/\text{Ce}^{4+}$ and Tb^{3+} in Ce/Tb co-doped $\text{Zn}_2(\text{BO}_3)(\text{OH})_{0.75}\text{F}_{0.25}$ phosphor: luminescence and energy transfer, *Adv. Powder Technol.* 30 (2019) 974–982.
- [48] S. Stojadinović, R. Vasilčić, Photoluminescence of Ce^{3+} and $\text{Ce}^{3+}/\text{Tb}^{3+}$ ions in Al_2O_3 host formed by plasma electrolytic oxidation, *J. Lumin.* 203 (2018) 576–581.
- [49] A.C. Yanes, J. del-Castillo, E. Ortiz, Energy transfer and tunable emission in BaGdF_5 : RE^{3+} (RE = Ce, Tb, Eu) nano-glass-ceramics, *J. Alloys Compd.* 773 (2019) 1099–1107.
- [50] X. Wu, Y. Jiao, O. Hai, Q. Ren, F. Lin, H. Li, Photoluminescence, energy transfer, color tunable properties of $\text{Sr}_3\text{La}(\text{BO}_3)_3$: Ce, Tb phosphors, *J. Alloys Compd.* 730 (2018) 521–527.
- [51] F. Xu, B. Zheng, H. Xia, J. Wang, B. Chen, Ratiometric temperature sensing behavior of dual-emitting $\text{Ce}^{3+}/\text{Tb}^{3+}$ co-doped $\text{Na}_5\text{Y}_2\text{F}_{13}$ single crystal with high relative sensitivity, *J. Alloys Compd.* 873 (2021) 159790.
- [52] S.K. Gupta, Z. Saikh, K. Sudarshan, K. Bhattacharyya, R.M. Kadam, Doped lanthanum cerate pyrochlore for multicolor luminescent phosphor: decisive role of energy transfer and defects, *J. Lumin.* 236 (2021) 118072.
- [53] H. Li, Y. Liang, S. Liu, W. Zhang, Y. Bi, Y. Gong, Y. Chen, W. Lei, Highly efficient green-emitting phosphor $\text{Sr}_4\text{Al}_{14}\text{O}_{25}$: Ce, Tb with low thermal quenching and wide color gamut upon UV-light excitation for backlighting display applications, *J. Mater. Chem. C* 9 (2021) 2569–2581.
- [54] J. Zhao, Y. Liang, G. Li, G. Wang, J. Ma, G. Dong, F. Wang, D. Wang, X. Li, From blue to cyan emission: Ce^{3+} and Tb^{3+} co-doped silicon phosphate phosphors with high thermal stability, *Phys. Chem. Chem. Phys.* 22 (2020) 9414, 9505.
- [55] S. Arrhenius, Über die dissociationswärme und den einfluss der temperatur auf den dissociationsgrad der electrolyte, *Z. Phys. Chem.* 4U (1889) 96–116.
- [56] X. Zhang, Y. Huang, M. Gong, Dual-emitting Ce^{3+} , Tb^{3+} co-doped LaOBr phosphor: luminescence, energy transfer and ratiometric temperature sensing, *Chem. Eng. J.* 307 (2017) 291–299.
- [57] E. Hertle, J. Bollmann, S. Assmann, V. Kalancha, A. Osvet, M. Batentschuk, S. Will, L. Zigan, Characterization of the phosphor $(\text{Sr,Ca})\text{SiAl}_3\text{Eu}^{2+}$ for temperature sensing, *J. Lumin.* 226 (2020) 117487.